Hindawi
Advances in Astronomy
Volume 2019, Article ID 2350476, 8 pages
https://doi.org/10.1155/2019/2350476

Research Article

Disk-Integrated Lunar Brightness Temperatures between 89 and 190 GHz

Martin J. Burgdorf,[1] **Stefan A. Buehler**,[1] **Imke Hans**,[2] **and Marc Prange**[1]

[1] *Universität Hamburg, Faculty of Mathematics, Informatics and Natural Sciences, Department of Earth Sciences, Meteorological Institute, Bundesstraße 55, 20146 Hamburg, Germany*
[2] *EUMETSAT, Eumetsat Allee 1, 64295 Darmstadt, Germany*

Correspondence should be addressed to Martin J. Burgdorf; martin.burgdorf@uni-hamburg.de

Received 30 November 2018; Revised 7 March 2019; Accepted 2 May 2019; Published 2 June 2019

Guest Editor: Zhiguo Meng

Measurements of the disk-integrated brightness temperature of the Moon at 89, 157, 183, and 190 GHz are presented for phase angles between -80° and 50° relative to full Moon. They were obtained with the Microwave Humidity Sounder (MHS) on NOAA-18 from 39 instances when the Moon appeared in the deep space view of the instrument. Polynomials were fitted to the measured values and the maximum temperature and the phase angle of its occurrence were determined. A comparison of these results with the predictions from three different models or rather parametrical expressions by Keihm, Mo & Kigawa, and Yang et al. revealed significantly larger phase lags for the lower frequencies in the measurements with MHS. As the Moon has appeared thousands of times in the field of view of all microwave sounders combined, this investigation demonstrates the potential of weather satellites for fine tuning models and establishing the Moon as extremely accurate calibration reference.

1. Introduction

In the year 1998 the first member of the fifth generation of satellites for Earth observation on polar orbits was launched by the National Oceanic and Atmospheric Administration (NOAA): NOAA-15. It carried two new microwave instruments, viz., AMSU-A and AMSU-B (Advanced Microwave Sounding Unit-A/B). When analyzing the data of AMSU-A, it became apparent that the calibration of this instrument is occasionally corrupted by the presence of the Moon in its field of view [1]. This is because AMSU-A points during every scan not only at Earth but also at an internal calibration target (ICT) of known temperature and into deep space. An interpolation between the counts from either reference source allows the calculation of the flux received from the Earth scenes. Sometimes it happens that the Moon is at the very position in the sky where AMSU-A or –B is observing space as cold reference for calibration (see Figure 1). As the instrument receives in this case the radiation of the Moon on top of the cosmic background radiation, it produces too high an output signal, which causes on its part a too low value for the gain of the receiver.

Mo & Kigawa [1] derived an effective brightness temperature (T_B) of the Moon as a function of phase angle from the intrusions of the Moon in the deep space view (DSV) of AMSU-A on NOAA-18. Their (4) is a rather rough approximation, where the disk-integrated T_B is the same for all frequencies, and it reaches its maximum value at full Moon. Since the 1960s, however, it is known that the maximum temperature of the Moon as measured in the wavelength range between 0.4 and 9.6 cm, corresponding to the frequency range 75-3.1 GHz, has a significant phase shift [2]. It is due to the fact that the radiation does not originate in the top layer of the surface, but it is rather emitted from a depth of tens of cm, where the heating from the Sun is delayed. AMSU-A covers a frequency range of 23.8–89 GHz; i.e., the phase shift found with ground-based observations of the Moon should be present in the data from the satellite as well.

Yang et al. [4] carried out a similar investigation with the Advanced Technology Microwave Sounder (ATMS) on the SNPP (Suomi National Polar-orbiting Partnership) satellite. They found a somewhat different relationship between phase angle and brightness temperature, which they assumed to

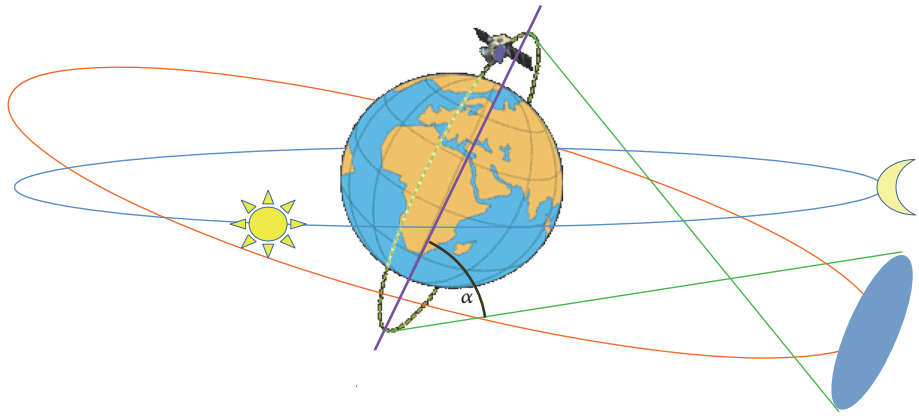

Figure 1: Pointing direction of the deep space view (green) compared to the celestial equator (red) and the ecliptic (blue). The slight tilt of the Moon's orbit against the ecliptic and of the orbital axis of the weather satellite against the equator is not shown for the sake of simplicity. The DSV points some 75° away from nadir—angle α in (3)—and describes a circle in the sky during an orbit of the satellite. When the Moon touches this circle, it appears in the DSV [3].

reach its maximum, however, again at full Moon. An important detail of these investigations is that the observations of the Moon were limited in both cases to phase angles φ between -75° and -60° relative to the full Moon. The reason is that both NOAA-18 before the year 2008 and SNPP crossed the equator in northern direction at about 13:30 local time. As the Moon can only appear in the DSV when it is positioned close to the orbital axis of the artificial satellite and more than 90° away from the Sun, the equator crossing time puts a tight constraint on the phase angles suitable for observation. This is shown schematically in Figure 1.

NOAA-18 changed its local equator crossing time between the years 2008 and 2018 by more than six hours. This peculiarity makes it possible now to calculate the brightness temperature of the Moon over a range of phase angles larger than 125° by analyzing its intrusions in the DSV of MHS (Microwave Humidity Sounder) on this satellite. As these measurements were carried out with both waxing and waning Moon, they allowed determining the phase angle of maximum brightness temperature with high accuracy for all channels of MHS, i.e., 89, 157, 183, and 190 GHz.

2. Materials and Methods

2.1. Identification of Moon's Presence in the Centre of the DSV. The first step on the way of calculating the brightness temperature of the Moon was to find its intrusions in the DSV of MHS on NOAA-18. Compared to other microwave sounders and other satellites, this one is particularly suited for this purpose because of the following reasons:

(i) MHS on NOAA-18 is recommended by FIDUCEO (http://www.fiduceo.eu) (FIDelity and Uncertainty of Climate data records from Earth Observations) and GSICS (https://gsics.wmo.int/en/welcome) (Global Space-based Inter-Calibration System) for use as reference instrument. Systematic calibration errors of other instruments are identified by comparison to this one. This means that the photometric stability of MHS on NOAA-18 is very high.

(ii) NOAA-18 was launched on May 20, 2005. All channels of MHS on this satellite worked flawlessly until 20 October 2018, when the scan mechanism failed.

(iii) As mentioned above, NOAA-18 turned from an afternoon to a morning satellite. This means that NOAA-18 provided data from a large range of phase angles around full Moon.

(iv) MHS has a smaller field of view than AMSU-A and therefore achieves a better signal-to-noise ratio with its observations of the Moon.

The method for identifying the Moon intrusions in the DSV was described in detail in Burgdorf et al. [5]. It starts with calculating the minimum distance between the pointing direction of the DSV and the position of the Moon for all orbits of the whole mission with a program called mhscl that is part of AAPP (ATOVS [Advanced TIROS {Television and Infrared Observation Satellite} Operational Vertical Sounder] and AVHRR [Advanced Very High Resolution Radiometer] Pre-processing package). In the first step, events, where this distance is a small fraction of a degree, are selected. There is an uncertainty, however, of about 0.3° in the calculated pointing direction and a discrepancy of similar size in the alignment of the different channels [6]. Hence, in the second step, we have taken advantage of the fact that in every scan there are four measurements of the signal from deep space at slightly different directions, each of them with its own "light" curve, i.e., the signal s as a function of time t as the DSV moves over the Moon in the cross-scan direction (see Figure 1 in [6]). Considering those intrusions, where the Moon gave the maximum signal in the DSV pixel with number $n = 2$ or 3, and identifying those instances, where it gave almost the same signal in the neighbouring DSV pixels n-1 and n+1, we obtained a collection of events, where the Moon came closer than 0.1° to the centre of DSV n. This way we made sure that the maximum signal was measured with

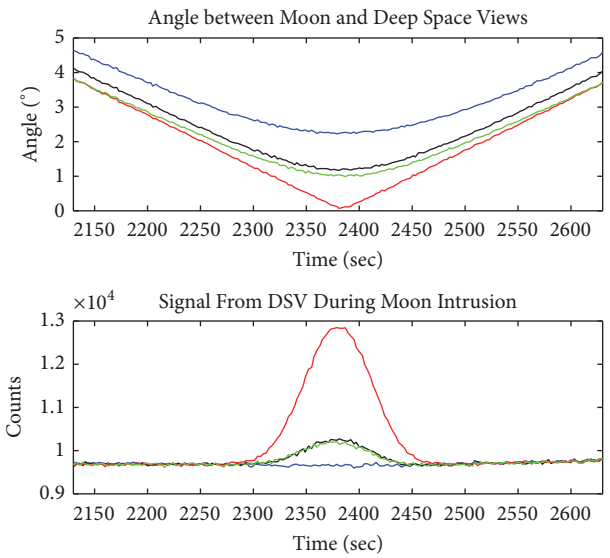

FIGURE 2: Moon intrusion event in different deep space views on 15 November 2010, with channel H1 of MHS on NOAA-18; blue: DSV 1; black: DSV 2; red: DSV 3; green: DSV 4. Top: angle between Moon and space view as calculated with AAPP. Bottom: space view counts. The time is given in seconds after 17:23 UT, the time of the first scan in the raw data file (level 1b). The angles calculated with AAPP are not quite accurate, and this is why DSV 2 gives a slightly larger signal than DSV 4 [7].

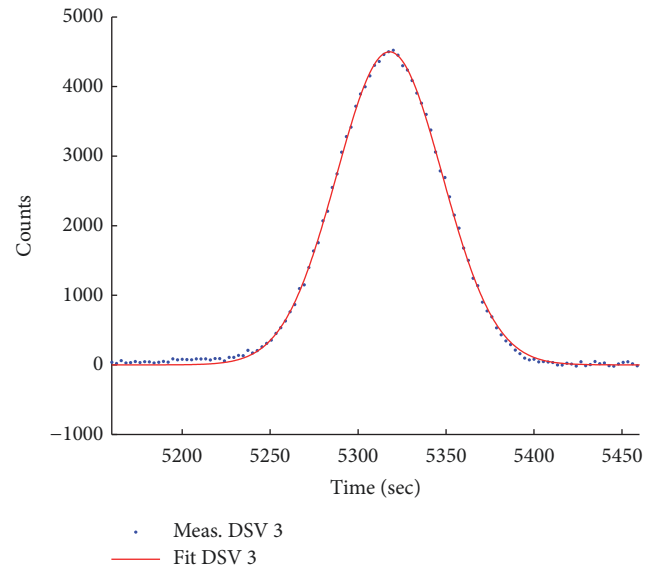

FIGURE 3: Moon intrusion event in deep space view 3 on 29 September 2018 (last Moon intrusion considered), with channel H1 of MHS on NOAA-18; blue dots: measured signal from each scan; red line: Gaussian fit to the measured points. The "light" curve resembles very closely a Gaussian.

the Moon always at the same position in the beam pattern (see Figure 2).

2.2. Evaluation of the "Light" Curve Produced by the Presence of the Moon in the DSV. The "light" curve can be well fitted with a Gaussian in MATLAB (see Figure 3):

$$s = ae^{-((t-b)/c)^2} \tag{1}$$

where a is the amplitude, b is the centroid (Moon closest to centre of DSV), and c is related to the peak width. The relationship between c and the full duration at half maximum ($FDHM$) of the intrusion of the Moon in the DSV is

$$FDHM = 2\sqrt{\ln 2}c \tag{2}$$

a is the number of counts when the Moon is closest to the centre of the beam.

As the reference sources used for calibration—the internal blackbody and the cosmic microwave background—are quite extended, while the Moon fills only a fraction of the field of view of MHS, it is necessary to know the beam size with high accuracy. The full width at half maximum ($FWHM$) has been measured during the ground tests of MHS at DASA with an alleged accuracy of 0.01°, according to [8]. Employing these values in the calculation of the brightness temperature of the Moon, however, produces discrepancies between the sounding and the window channels too large to be explained by the differences in frequency (the $FWHM$ claimed by DASA implies a *maximum* disk-integrated T_B^{Moon}, i.e., soon after full Moon, of only 210 K at 183 GHz). We have therefore determined $FWHM_{ch}$ for each channel of MHS from the width of the Gaussians fitted to the "light" curve of the Moon intrusions in the DSV. The relationship between these physical quantities is

$$FWHM_{ch} = \frac{360^\circ \cdot 2 \cdot \sqrt{\ln 2} \cdot c \cdot \cos\alpha}{P} \tag{3}$$

The elements of this equation are defined as follows:

(i) α = angular distance between the pointing direction of the DSV and the orbital plane of NOAA-18 (72.1° for pixel 1, 73.2° for pixel 2, 74.3° for pixel 3, 75.4° for pixel 4, the orientation of the DSV is always away from the Sun, see Figure 1);

(ii) P = orbital period of NOAA-18 (6078 sec).

Equation (3) is basically the same as the second equation in [9], with an orbital angular velocity of $360^\circ \cos\alpha / P$ and the peak width replacing the channel displacement.

We assume in the following that the beam of MHS is rotationally symmetric; i.e., that the FWHM we have determined in the cross-scan direction is the same as the FWHM in the scan direction, which one cannot determine with high accuracy from the Moon intrusions. This assumption is justified by the characterization of the shape of the beam that was carried out on ground [8].

Equation (3) might slightly overestimate $FWHM_{ch}$, because the Moon is an extended source and has therefore a longer presence in the DSV than a point-like object. As the diameter of the Moon is less than half the FWHM (or Θ_{3dB}, as it is called in the reports of the ground tests) of the beam of MHS (see Table 1), however, and the origin of its flux is concentrated in the warmest region of its surface

Table 1: Antenna performance—space view—centre frequencies (values from [8], except for the last column, where values were calculated for a point-like lunar emission and, in brackets, a $FWHM_{Moon}$ of 0.4°).

Channel	Ground test frequency [GHz]	Beam efficiency	Θ_{3dB}[°] (ground test)	Θ_{3dB}[°] (Moon)
H1	89.3	0.941±0.001	1.09±0.01	1.20(1.13)±0.02
H2	157.3	0.997±0.001	1.03±0.01	1.09(1.01)±0.02
H34	184.3	0.971±0.001	1.05±0.01	1.25(1.18)±0.01
H5	190.6	0.961±0.001	1.05±0.01	1.27(1.20)±0.01

(see, for example, figures in [10]), any systematic error in (3) must be small. We assume $FWHM_{Moon} = 0.4°$ for the radiance distribution of the lunar disk. This value is representative for phases close to full Moon, at quarter Moon it would be smaller. The values for $(FWHM_{ch}{}^2 - FWHM_{Moon}{}^2)^{0.5}$, i.e., the beam size after correction for the fact that it was determined with an extended source instead of a point source, are given in brackets in the last column of Table 1. Only $FWHM_{Moon} \approx 0.4°$ results in beam sizes that are compliant with specifications ($1.1° \pm 0.11°$) for each channel. But whatever the error of our value for Θ_{3dB} is, it is the same for all measurements and does therefore not affect the ratio between brightness temperatures at different phase angles.

2.3. Calibration of the Measurements Made with the DSV of MHS on NOAA-18. As intrusions of the Moon in the DSV are not suitable for the standard processing of data obtained with MHS, we started the calculation of brightness temperatures with the output signal expressed in digital counts that is available in the level 1b database. A polynomial of degree two was fitted to the counts from the DSV as a function of time before and after the appearance of the Moon and then used to calculate the counts that would have been obtained, if the Moon had not been present, i.e., only from the cosmic microwave background. These counts and the ones obtained on the ICT in combination with the known temperatures of the cosmic microwave background and the ICT were then used to calculate a linear relationship between counts and spectral radiance. A "cold load correction factor" of 0.24 K, as given in the file mhs_clparams.dat of AAPP, was added. No warm load or band correction was applied, because they were considered negligible on the basis of the values given in AAPP. See [11] for a detailed discussion of these and other instrumental effects.

The Gaussian is fitted to the light curve of the Moon in counts from the DSV after subtraction of the "baseline" with the polynomial determined in the previous step. This way not only the contribution from the cosmic microwave background is removed, but also the slightly variable thermal emission from the mirror [12] and the platform. It can be seen from Figure 2, where the raw counts before subtraction of the baseline flux are plotted, that the in-orbit variations are quite small and variable on time scales much larger than the duration of the Moon intrusion. Every light curve we used was carefully inspected for sudden jumps in the counts, which, however, happened only very rarely.

The amplitude of the Gaussian fit is divided by the gain of the relevant channel and the fraction of the field of view covered by the Moon, under the assumption that the beam can be described by a two-dimensional Gaussian function, and the Moon moves through the centre of the pixel. In this case the fraction of the beam covered by the Moon F_{ch} follows from (1) by replacing time with distance from the centre of the beam r and integration of the beam pattern over the area covered by the Moon:

$$F_{ch} = \frac{1}{2\pi} \int_0^{r_{Moon}/c} \int_0^{2\pi} e^{-r^2/2} r \, d\omega \, dr = -\left[e^{-r^2/2}\right]_{r=0}^{r_{Moon}/c} \quad (4)$$

2π is the value of the integral with upper border $r = \infty$. Equation (4) is only valid at one point of the "light" curve: its maximum. With F_{ch} it is possible to calculate the spectral radiance of the Moon:

$$B_\nu^{Moon} = \frac{a}{G\eta F_{ch}} + B_\nu^{CMB} \quad (5)$$

The elements of these equations are defined as follows:

(i) $B_\nu{}^{Moon/CMB}$ = spectral radiance of the Moon/cosmic microwave background;

(ii) G = gain of the instrument in counts per unit of spectral radiance;

(iii) η = beam efficiency as measured on ground [8];

(iv) F_{ch} = fraction of the beam covered by the Moon = $e^{4 \ln 2 r_{Moon}^2 / FWHM_{ch}^2} - 1$, derived from (2) and (4);

(v) r_{Moon} = radius of the Moon as seen from the spacecraft at the time of maximum signal.

F_{ch}, just like G and η, takes slightly different values with different channels, except for three and four, which share the same "quasi-optical" path in MHS.

Equation (5) contains a term to correct for the part of the cosmic microwave background being blocked by the Moon, when an intrusion happens. It is needed, because the full microwave background was subtracted before the amplitude a of the "light" curve was calculated; see Figure 3. This way we make sure that $B_\nu{}^{Moon}$ cannot be negative, even in the hypothetical case of a Moon that does not emit any microwaves. The resulting spectral radiance is then converted to the brightness temperature of the Moon with an inverse Planck function.

3. Results and Discussion

3.1. Brightness Temperatures as a Function of Phase Angle. The brightness temperatures calculated with (5) and the inverse Planck function are plotted as a function of phase angle in

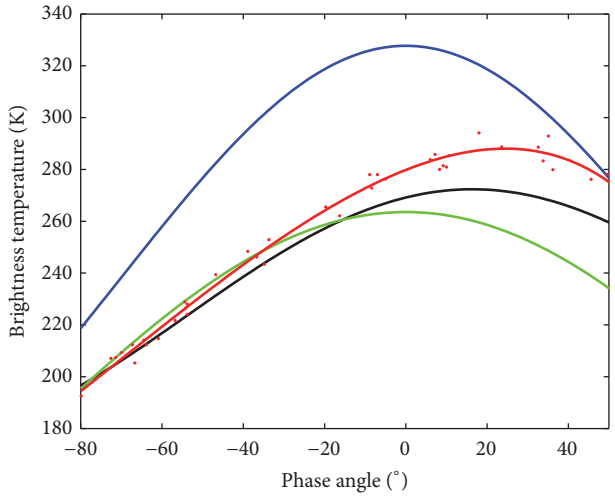

Figure 4: Disk-integrated brightness temperatures of the Moon for different phase angles relative to full Moon at 89 GHz. Blue: (4) in [1], green: (4) and Table II in [4], black: Keihm ([13], numbers from web page and personal communication), and red: MHS on NOAA-18, single measurements (dots) fitted with polynomial of order five.

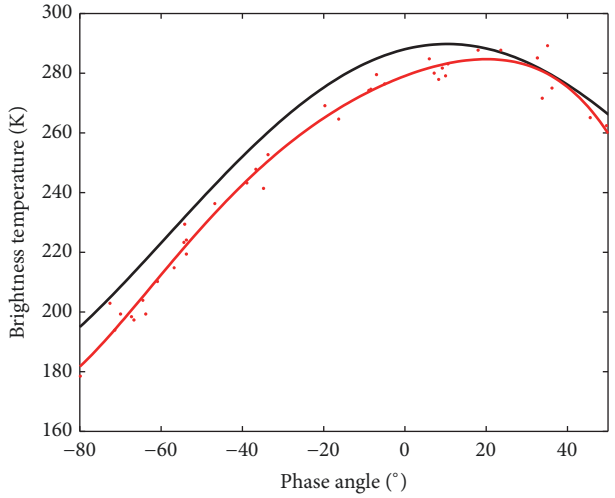

Figure 5: Disk-integrated brightness temperature of the Moon for different phase angles relative to full Moon at 157 GHz. Black: Keihm ([13], numbers from web page and personal communication); red: MHS on NOAA-18, single measurements (dots) fitted with polynomial of order five.

Figures 4–6. A polynomial of degree five was fitted to the measured values and is shown together with the predictions of three different models. These models are as follows:

(i) Keihm [13]: a lunar regolith model, including depth and temperature dependencies of the relevant thermal and electrical properties, whose brightness temperatures are available on a web page (http://lunar-model-brightness-temperatures.net) or by request.

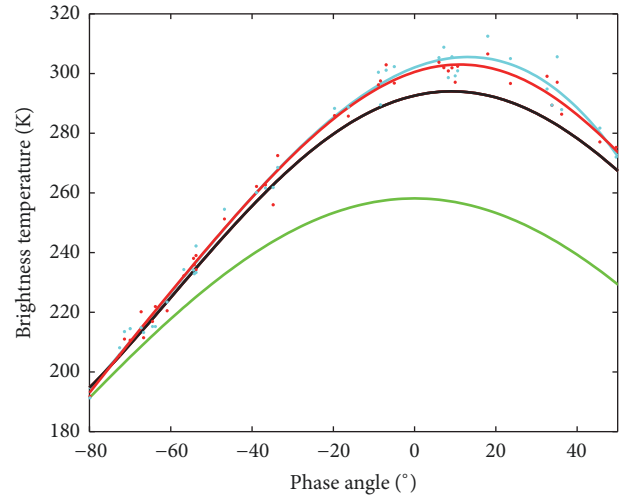

Figure 6: Disk-integrated brightness temperature of the Moon for different phase angles relative to full Moon. Green: Equation (4) and Table II in [4], 183.3 GHz, black: Keihm ([13], numbers for 183.3 GHz from web page and personal communication), red: MHS on NOAA-18, 183.3 GHz, and cyan: MHS on NOAA-18, 190.3 GHz, single measurements (dots) fitted with polynomial of order five.

(ii) Mo & Kigawa [1]: a simple expression for the effective lunar surface brightness temperature for correcting the lunar contamination in AMSU-A data.

(iii) Yang et al. [4]: a polynomial of degree two in $\cos\varphi$, similar to the one employed by Mo & Kigawa that is based on observations from the Diviner Lunar Radiometer Experiment and takes a wavelength-dependent surface emissivity of the Moon's disk into account.

According to (4) in [1], the effective Moon brightness temperature is the same for all channels of AMSU-A, i.e., in the range 23.8–89 GHz. As this assumption is certainly not valid for higher frequencies [14], we have plotted the values from this model only in Figure 4. The surface emissivity is, however, a factor in (4) of [4] and was therefore calculated for both channels that ATMS has in common with MHS, i.e., at 89 and 183.3 GHz.

The measured values for the brightness temperature in different channels and at different lunar phases, shown as dots in Figures 4–6, have uncertainties that can be calculated from the random scatter around the polynomial fit. We obtained a standard deviation of 3.2 K for the measurements in channel 1, 4.1 K for channel 2, 3.8 K for the average of channels 3 and 4, and 5.1 K for channel 5. These values are significantly larger than the noise of the receivers alone [15], given the fact that each point in the plots is the result of a Gaussian fit to measurements from about 100 different scans (see Figure 3). But it is only the measurements near the centroid that strongly constrain the amplitude of this fit, and even small outliers in the raw data can introduce an error.

A correlation of the scatter of the measurements with the liberation of the Moon or its distance from the Sun could not be found. If such a dependency exists, it must be negligible compared to the random uncertainty of the measurements.

Table 2: Maximum brightness temperature of the Moon at different frequencies and the phase of its occurrence.

Source	T_{89} [K]	Φ_{89}	T_{157} [K]	Φ_{157}	T_{183} [K]	Φ_{183}
Keihm	272±14	16°	290±15	10°	294±15	9°
Mo & Kigawa	328	0°	-	-	-	-
Yang et al.	264	0°	-	-	255	0°
MHS on N-18	288±4	24°	285±6	20°	303±5	11°

3.2. Main Features of the Measurements with MHS on NOAA-18 and Models. The relationship between the brightness temperature of the Moon and its phase as given by the measurements with MHS and the models is characterized by two key quantities: the maximum brightness temperature, averaged over the disk, and the phase lag between full Moon and the occurrence of this maximum temperature. Table 2 gives an overview of these values.

The uncertainties of the measured brightness temperatures in Table 2 were calculated from the scatter of the values for the diameter of the beam of each channel that were determined from the Moon intrusions in the DSV themselves, as explained above. The beam efficiency η, which is an expression for the losses of the main beam due to side lobes and which we took at face value from [8], contributes an additional, systematic uncertainty to the brightness temperatures measured with MHS. It should be less crucial than the uncertainty of the beam width, however, because η must be close to one and does not enter the calculation of the radiance in quadrature. The absolute uncertainty of the Apollo-based model predictions was calculated on the basis of the estimate given on Keihm's web page.

All things considered there are no significant differences between the maximum brightness temperatures obtained with MHS and the model by Keihm [13]. The mathematical expression given by Yang [4] for the maximum brightness temperature of the disk-integrated Moon, however, is not compatible with the values obtained with MHS on NOAA-18 at 183 GHz, and the same is true for the estimate provided by Mo & Kigawa [1] at 89 GHz.

With respect to the phase shift between full Moon and the time of maximum microwave brightness temperature, the measurements with MHS gave significantly higher values than all models, except for the one by Keihm at 183 GHz. It is noted that assuming a different beam diameter or efficiency has almost no effect on the phase lags measured with MHS, since they affect essentially all measurements the same way. Because of the excellent stability of MHS on NOAA-18 [16], the uncertainty of the phase lags is mainly due to the random scatter of the measurements.

4. Conclusions

Our investigation has produced two major, new findings:

(1) The difference in beam size between the sounding channels and H2 is almost ten times as large as the value measured with the ground tests that were supposed to demonstrate the compliance with the requirements for MHS on NOAA-18. This is of particular relevance for the verification and check out of MHS on Metop-C, which was launched on 7 Nov 2018, because it shows that the beam size has to be verified in flight.

(2) The phase angle of the Moon, where the disk-integrated brightness temperature reaches its maximum, is at the lower frequencies larger than each of the models predicted, hence they do not reproduce the difference between waxing and waning Moon correctly. This is particularly relevant for the model by Keihm, because it is supposed to be used for the calibration of astronomical observations.

On top of that our investigation demonstrates that precise measurements from weather satellites can provide useful information also about objects other than Earth.

At 183.3 GHz, the frequency of the H_2O absorption at the $3_{1,3} \longrightarrow 2_{2,0}$ resonance, there is agreement within the margins of uncertainty between the observations with MHS and the model by Keihm. This confirms the validity of the method employed to turn raw data from the deep space view into brightness temperatures. By the same token it is an additional proof for the existence of the microwave phase lag, which is absent in those functions relating T_B^{Moon} to phase angle φ that are based on observations over only a narrow range of phase angles at waxing Moon. One cannot identify the phase angle of maximum brightness temperature solely on the basis of the measurements presented in [1, 4]. The model by Yang et al., however, agrees with the values given by Keihm in the range φ = -70°± 10° and has the advantage of a simple mathematical relationship between brightness temperature and phase angle, which makes it attractive for applications involving the processing of large amounts of data from afternoon satellites. Such applications are, for example, the removal of the contamination of the counts from the DSV by the presence of the Moon or checks of the stability of the photometric calibration [1, 4]. The model by Yang is based on actual measurements with ATMS at phase angles between -75° and -60° relative to the full Moon. Its very good agreement with the results we obtained with MHS at the same phases is proof of the high accuracy of the brightness temperature values achievable by analyzing the Moon intrusions in the DSV of meteorological research satellites. It also demonstrates the relevance of the Moon for cross calibration, because it enables the detection of biases between quite different instruments operating at quite different times, a weighty prerequisite for studies of climate change with satellite data.

The main strength of the observations of the Moon with MHS lies in the determination of the microwave phase lag effect and the corresponding asymmetry between the

brightness temperatures of waxing and waning Moon. This is because its characterization relies on differences between measured fluxes and not their absolute values so that most of the possible systematic errors, related, for example, to properties of the beam, cancel out. The fact that the phase lag found with the window channels of MHS is significantly larger than the one predicted by the models suggests that the thermophysical and electrical properties of the bulk regolith are not identical with the values derived from the returned Apollo samples.

This finding is important, because the Moon has been used as calibration reference by a large number of astronomical microwave projects, where assuming a wrong phase lag causes systematic errors. Interestingly enough a two-week, 5% lunar phase-dependent error appeared in the calibration of COBE (COsmic Background Explorer) at 53 GHz, when the brightness temperature of the Moon was calculated with Keihm's model [17]. The uncertainty of the phase lag can be reduced by analyzing more than the 39 intrusions of the Moon in the DSV that are the basis of the numbers given in Table 2. The Moon appeared altogether 1566 times in the DSV of MHS on NOAA-18 between May 2005 and October 2018, and this number is similar for other satellites. The uncertainty of the maximum brightness temperature of the Moon can be reduced by analyzing data from more satellites: there are five MHSs and three AMSU-Bs in orbit, and averaging their measurements would significantly mitigate the impact of systematic errors.

Taking advantage of the Moon as calibration reference is not limited to the microwave range of the spectrum. The Earth and the Moon are, for example, the only targets observed during the cruise phase of Hayabusa2, which can be used as calibrators for the TIR (Thermal InfraRed imager) [18]. As there are numerous instruments on satellites for Earth observation with mid-infrared channels, an accurate characterization of the lunar radiance in the infrared could be achieved by using a method analogous to the one described in this article for MHS.

Data Availability

The level 1b data from MHS presented in this manuscript are available from NOAA CLASS (Comprehensive Large Array-data Stewardship System).

Conflicts of Interest

The authors declare that they have no conflicts of interest.

Acknowledgments

The authors would like to thank Oliver Lemke for making the satellite data available and Roberto Bonsignori for providing information about MHS on NOAA-18. The characterization of the Moon as flux reference is part of an effort to quantify the uncertainty budget for microwave sounders undertaken within the H2020 project, Fidelity and Uncertainty in Climate data records from Earth Observation (FIDUCEO). FIDUCEO has received funding from the European Union's Horizon 2020 Programme for Research and Innovation, under grant agreement no. 638822.

References

[1] T. Mo and S. Kigawa, "A study of lunar contamination and on-orbit performance of the NOAA 18 advanced microwave sounding unit–A," *Journal of Geophysical Research: Atmospheres*, vol. 112, no. D20, 2007.

[2] V. D. Krotikov and V. S. Troitskiĭ, "Radio Emission and Nature of the Moon," *Soviet Physics Uspekhi*, vol. 6, no. 6, pp. 841–871, 1964.

[3] M. Burgdorf, S. A. Buehler, T. Lang, S. Michel, and I. Hans, "The Moon as a photometric calibration standard for microwave sensors," *Atmospheric Measurement Techniques*, vol. 9, no. 8, pp. 3467–3475, 2016.

[4] H. Yang, J. Zhou, F. Weng et al., "Developing vicarious calibration for microwave sounding instruments using lunar radiation," *IEEE Transactions on Geoscience and Remote Sensing*, vol. 56, no. 11, pp. 6723–6733, 2018.

[5] M. Burgdorf, I. Hans, M. Prange, T. Lang, and S. A. Buehler, "Inter-channel uniformity of a microwave sounder in space," *Atmospheric Measurement Techniques*, vol. 11, no. 7, pp. 4005–4014, 2018.

[6] R. Bonsignori, "In-orbit verification of microwave humidity sounder spectral channels coregistration using the moon," *Journal of Applied Remote Sensing*, vol. 12, no. 02, 2018.

[7] M. Burgdorf, T. Lang, and S. Michel, "The Moon as a diagnostic tool for microwave sensors," *GSICS Quarterly*, vol. 10, 2016.

[8] C. A. Whatling, "Microwave Humidity Sounder Instrument End Item Data Package PFM Model," *Matra Marconi Space*, vol. 3, no. 2, 1999, https://www.eumetsat.int/website/home/Satellites/CurrentSatellites/Metop/MetopDesign/MHS/index.html.

[9] R. Bonsignori, "In-orbit verification of MHS spectral channels co-registration using the moon," in *Proceedings of the SPIE*, vol. 10402, 2017.

[10] R. J. Coates, "Note: lunar brightness variations with phase at 4.3-MM wave length," *The Astrophysical Journal*, vol. 133, 1961.

[11] I. Hans, M. Burgdorf, S. Buehler, M. Prange, T. Lang, and V. John, "An uncertainty quantified fundamental climate data record for microwave humidity sounders," *Remote Sensing*, vol. 11, no. 5, 2019.

[12] H. Yang, F. Weng, and K. Anderson, "Estimation of ATMS antenna emission from cold space observations," *IEEE Transactions on Geoscience and Remote Sensing*, vol. 54, no. 8, pp. 4479–4487, 2016.

[13] S. J. Keihm, "Interpretation of the lunar microwave brightness temperature spectrum: feasibility of orbital heat flow mapping," *Icarus*, vol. 60, no. 3, pp. 568–589, 1984.

[14] J. G. Mangum, "Main-beam efficiency measurements of the Caltech Submillimeter Observatory," *Publications of the Astronomical Society of the Pacific*, vol. 105, 1993.

[15] I. Hans, M. Burgdorf, V. O. John, J. Mittaz, and S. A. Buehler, "Noise performance of microwave humidity sounders over their lifetime," *Atmospheric Measurement Techniques*, vol. 10, no. 12, pp. 4927–4945, 2017.

[16] I. Moradi, J. Beauchamp, and R. Ferraro, "Radiometric correction of observations from microwave humidity sounders," *Atmospheric Measurement Techniques*, vol. 11, no. 12, pp. 6617–6626, 2018.

[17] C. L. Bennett, G. F. Smoot, M. Janssen et al., "COBE differential microwave radiometers," *Astrophyscial Journal*, vol. 391, 1992.

[18] A. Matsuoka, C. T. Russell, S. Tanaka et al., ""Earth and moon observations by thermal infrared imager on Hayabusa2 and the application to detectability of asteroid 162173 Ryugu," *Planetary and Space Science*, vol. 158, 2018.